

83-37
N93-103947

An Experimental Technique For Performing
3-D LDA Measurements Inside
Whirling Annular Seals

p. 7

by

Gerald L. Morrison

Mark C. Johnson

Robert E. DeOtte, Jr.

H. Davis Thames III

Brian G. Wiedner

Mechanical Engineering Department

Turbomachinery Laboratory

Texas A&M University

College Station, Texas 77843

Presented at

Sixth International Symposium On Application

Of Laser Techniques To Fluid Mechanics

July 20-23, 1992

Lisbon, Portugal

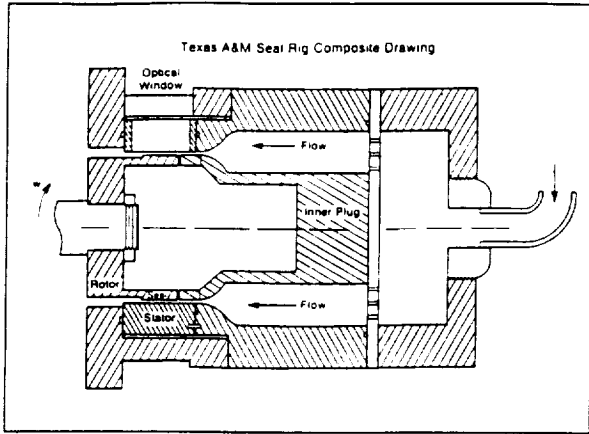


Figure 2 Seal Test Facility Schematic.

can be cantilever mounted from the perforated plate. The purpose of the plug and the contoured outer walls is to smoothly accelerate the fluid into the seal. An additional axisymmetric ring possessing small vanes can be mounted on the downstream end of the plug (just upstream of the rotor) to provide a known amount of preswirl to the fluid.

Water is supplied to the test apparatus by a 56 Kw (75 Hp) centrifugal pump via a turbine meter and throttling valve which are used to establish and maintain the flow rate. The water exiting the test apparatus is returned to a 15 m³ (4,000 gallon) reservoir. The LDA system requires seed particles in the water. Expancel 461 was used (about a tea cup full) which has a specific gravity of 1.29 and a mean diameter of 6 μm ± 0.2 μm. This particle has a frequency response of 44 KHz in water which was deemed sufficient for the present study.

The particular annular seal being discussed in this paper is constructed of acrylic and has a rotor (journal) diameter of 0.163 m, a length of 37.3 mm, and a nominal clearance of 1.27 mm. In the current arrangement, the centerline of the shaft upon which the rotor is mounted is offset from the centerline of the rotor by 0.63 mm resulting in an eccentricity ratio of 50% and a rotor which is whirling at the same speed as the shaft.

An optical window was installed such that the entire length of the seal can be measured. The optical window is constructed of quartz and has a trapezoidal cross section (3.55 mm wide at the bottom {bush} expanding to 18.8 mm wide at top {outside}) and is 62.23 mm long. The top and bottom of the window are flat and parallel to each other to eliminate optical distortion and any focusing effect of the window. This is essential for the six beam LDA system being used since any lens effect limits the ability to traverse the probe volume about the flow field without continual realignment. The present design results in acceptable beam coincidence being maintained over a penetration depth of about 4 times the clearance (in water). The flat bottom of the window causes an out of roundness of the bush which is 0.027% of the rotor radius or 1.5% of the clearance.

The rotor was manufactured of clear acrylic and polished to obtain a smooth surface. The purpose of using acrylic is to reduce the amount of light reflected by the laser beams. This is very important in the present study since the laser beams must enter the test section along radial lines which produce significant amounts of flare (diffuse reflection) and specular reflection. In order to further minimize the light reflection an optical coating was applied to both the rotor and window. The quartz window's reflectance was decreased from 9.3% to 1.3% while the rotor's reflectance was decreased from 3.7% to 2% for 514.5 nm wavelength light. The rotor was coated using a special low temperature vacuum deposition technique.

Further considerations necessary to perform measurements inside the small gap (1.27 mm) included the orientation of the laser beams entering the test section. The natural tendency is to align the two optical trains symmetrically about the normal of the optical window. This generated a problem with specular light reflection from the window and rotor in that low power reflected beams were projected into the receiving optics and bounced around inside the optical train. This was unacceptable since the beam could hit the photomultiplier tube. Therefore, the LDA system was yawed with respect to the axial direction of the seal 9.8° so that reflected beams missed the receiving optics lenses. The yaw created a new problem in that the optical cone of light gathered by the receiving optics was distorted resulting in a blurred focal point. The greater the angle of yaw, the worse the distortion.

The alignment of the transmitting and receiving optics had to be done in situ due to the bending of the light as it traveled from the air into quartz and into water. The transmitting optics were aligned by using a 15 μm diameter high power pinhole mounted 0.63 mm (0.025") from the quartz window in the water. The high power pinhole was required so that heating by the laser beam did not cause distortion. Alignment was accomplished by blocking five of the beams and adjusting the remaining beam until it was centered in the pinhole. The beam was considered centered when a) maximum power was passing through the pinhole and b) the diffraction pattern generated by the beam passing through the pinhole was symmetric. Each beam was thus aligned through the pinhole assuring coincidence of the six beams at the probe volume.

The photomultiplier tubes were more difficult to align because the off-axis backscatter system results in a blurred side view of the probe volume. Additionally, the photodetector can be aimed at any location along the length of an individual probe volume (of which only 39% was located in the composite probe volume) and still receive valid Doppler bursts. In order to obtain coincident data, all three photodetector signals were displayed on a four channel oscilloscope. By triggering off the various photodetector signals, one can visually observe time lags between the Doppler bursts of the individual photodetectors. When all three photodetectors are focused on the same spatial location the time lags should be zero. This is evidenced by the presence of all three bursts occurring at the same time or at least within the 10 μs coincidence window used for these measurements.

The selection of the 10 μs coincidence window was determined by experimentally observing the correlation

coefficients $\left[\frac{u_i' u_j'}{\sqrt{u_i' u_i'} \sqrt{u_j' u_j'}} \right]$ between the various velocity

components measured directly by the LDA for various coincidence window settings. Morrison, et al. [1991a] showed that in isotropic turbulence the correlation coefficient should equal the cosine of the angle between the velocity components. Since our system is measuring non-orthogonal velocity components, the technique can be applied to our data. This criterion has been used in our laboratory for many years and has been invaluable in validating the operating parameters used on the LDA. It was found that coincidence window settings larger than 10 μs resulted in a decreased correlation coefficient indicating poor coincidence. If coincidence is poor, the transformation of the velocity measurements from the non-orthogonal to an orthogonal coordinate system will yield an incorrect "on-axis" (Z direction in Figure 1) velocity component and components of the Reynolds stress tensor will be incorrect.

The present set of measurements involves a whirling annular seal. This requires a rotary encoding system which tags each data point with the angle of the rotor. Previous work (Morrison, et al. [1991b]) in non-whirling seals required 2,000

velocity vector realizations at each spatial location to obtain repeatable mean velocity and Reynolds stress tensor values. With the addition of the azimuthal dependence in the data, 90,000 velocity vector realizations were recorded at each axial-radial location in the present study and the results phase averaged to obtain the mean velocity and Reynolds stress tensor at 18 shaft phase angles. The number of velocity realizations at each phase angle varied from 1000 to 9000. The rotary encoding system was directly interfaced to the three counter systems used to validate the Doppler bursts. The McLaughlin-Tiederman [1973] velocity bias correction scheme was used on all of the data. This technique is easily applied to the 3-D data since the magnitude of each instantaneous velocity realization is obtained by the 3-D LDA system.

RESULTS

Mean Velocity

The mean axial, radial, and azimuthal velocities are shown in Figures 3 and 4. The rotor is whirling (precessing) in a clockwise direction. Upstream and at the inlet to the seal (Figures 3 and 4) the flow vectors on the pressure side are pointing inward. Upstream of the seal at $Z/L = -0.02$ (Figure 4), the mean axial velocity profile reaches a peak of greater than $0.9U_{ave}$ (6.6 m/s, where $U_{ave} = 7.4$ m/s) between 60° and 135° . The radial velocities are generally pointed inward toward the seal because the flow has just been diverted inward by the curve in the plenum wall. The greatest inward mean radial velocities are located in the same region as the high U's. The inlet W does not exceed $0.08W_{sh}$ ($0.33U_{ave}$, 2.4 m/s) over most of the clearance.

At the seal inlet (Figure 3) the axial flow component begins to accelerate into the seal. The peak axial velocity is $1.5U_{ave}$ (11 m/s) across a band from 30° to 60° and stays above $0.5U_{ave}$ (3.7 m/s) across the entire circumference of the seal. The V profiles continue the strong inward trend. The maximum inward velocity reaches $-0.8U_{ave}$ (-6 m/s) from 45° to 190° . It appears that the inward momentum imparted to the flow by the curved stator wall is still affecting the fluid, but at the same time, the inlet shape of the seal is directing flow to the cavity under the seal. The tangential velocities begin to increase, with the $0.08W_{sh}$ (2.4 m/s) contour extending almost to the stator from 280° to 60° , and moving outward through the suction portion of the clearance.

Just downstream of the inlet at $Z/L = 0.04$ (Figure 4) the axial velocities are much greater, with a maximum of $2.2U_{ave}$ (16.3 m/s) occurring at 95° . This peak is very close to the stator, and there are very high $\partial U/\partial r$ gradients on either side of the peak. A shear layer exists from 90° to 180° . A mild recirculation zone exists between the rotor and the shear layer with a maximum backflow velocity of $-0.1U_{ave}$ (-0.7 m/s). This recirculation zone occupies less than 15% of the clearance and is not visible on the figures. Reattachment of the axial velocity occurs at 180° where the axial velocities are significantly smaller than on the other side of the clearance. The axial recirculation produces a small vena contracta. The V profile changes significantly at this point, as the direction of the velocities is redirected back out toward the stator. A maximum of $0.18U_{ave}$ (1.3 m/s) at 45° is surrounded by mild $\partial V/\partial r$ gradients on either side. The radial velocities are pointed outward near the rotor and inward near the stator on the wide clearance side of the rotor, indicating the presence of a vena contracta around 135° . Because the axial momentum in this area is so small, the tangential velocities are able to develop quickly, especially in the recirculation zone where $W = 0.24W_{sh}$ (6.9 m/s, $0.9U_{ave}$) in the middle of the clearance from 60° to 280° .

From $Z/L = 0.04$ to $Z/L = 0.07$ (Figure 4) the axial velocities decrease, only reaching a maximum of $1.9U_{ave}$ (14 m/s) at $\theta = 120^\circ$. The high velocity area is still along the stator, and

the steep $\partial U/\partial r$ gradients near the rotor surface are relaxing. The recirculation zone has disappeared along the rotor, but the velocities are still very low there. The disappearance of the shear layer implies that the axial streamlines have reattached to the rotor. The radial velocities are directed back out toward the stator after turning at the reattachment point. The tangential velocity development diminished with the reattachment of the axial velocity streamlines.

Moving to $Z/L = 0.14$ (Figure 4), the U profile is more evenly distributed throughout more of the seal, as the peak axial momentum region reaches wider clearances, which is decelerating the flow. The peak axial velocity is $1.5U_{ave}$ (11 m/s) and it is located at 90° . The rest of the profile remains attached to the rotor and stator with very mild $\partial U/\partial r$ gradients. The axial velocity on the suction side of the rotor is steadily increasing, with the minimum continuous contour at $0.7U_{ave}$, where just upstream it is $0.6U_{ave}$. The radial velocities continue to decrease in magnitude and now are fairly insignificant. The decrease in axial momentum is acting favorably for the tangential velocities, which are now increasing over the entire seal. The $0.08W_{sh}$ (2.4 m/s) level is now extending much further into the maximum clearance region, and it is distributed more uniformly.

From $Z/L = 0.14$ to $Z/L = 0.50$ (Figure 3) the trends discussed above continue; the axial velocity continues to spread more uniformly across the entire seal, the radial velocities remain small, and the tangential velocities increase with the decrease in axial momentum. At the midplane the axial velocity profile is almost uniform, with regions in the maximum clearance area having velocities which are a little higher. As the location of the maximum axial velocity rotates around the seal, the negative radial velocity zone also moves. By the midplane it is relocated to the minimum clearance region. The tangential velocity develops to $0.08W_{sh}$ all the way out to the stator, and it is increasing in the pressure section of the clearance, reaching $0.16W_{sh}$ (4.8 m/s) by the midplane.

Farther down the seal at $Z/L = 0.77$ the location of the maximum axial velocity is convected around the seal by the increasing tangential velocity component. The peak axial velocity is at 240° and has increased to $1.4U_{ave}$ (10.4 m/s) as the tangential component is forcing the fluid into a smaller region. The radial velocity is similar to that upstream, with positive values pointing out from the rotor and negative in from the stator. The tangential profile develops significantly, with the $0.24W_{sh}$ (6.9 m/s) zone extending almost entirely across the pressure zone around 60° . This significant increase in the tangential momentum is the mechanism driving the axial velocity peak around to the other side of the clearance.

The axial velocities on the suction side of the clearance continue to increase as the flow progresses downstream while the tangential velocities increase on the pressure side. This continues to the exit plane where the peak axial velocity reaches $1.7U_{ave}$ (12.6 m/s) at 265° . At the exit plane nearly the whole pressure side of the clearance is dominated by tangential velocities of at least $0.24W_{sh}$ (0.93U) and on the suction side they are $0.16W_{sh}$ (4.6 m/s). The radial profile remains virtually unchanged through the rest of the seal, not exceeding $0.08U_{ave}$ (0.6 m/s). The radial velocities are pointed inward along the stator.

Turbulence Levels

Upstream of the inlet, in the plenum at $Z/L = -0.02$ (Figure 4), the axial normal Reynolds stress term is extremely subdued, which is reflected in the mild gradients in the mean velocity terms. The $\overline{u'u'}$ term barely reaches more than $0.05U_{ave}^2$ ($2.7 \text{ m}^2/\text{s}^2$). At the inlet (Figure 3) the front edge of the rotor causes changes. The $\overline{u'u'}$ term builds (exceeding $0.33U_{ave}^2$, $18 \text{ m}^2/\text{s}^2$) along the rotor surface on the bottom side where the recirculation zone is located a bit farther downstream.

(Note: the recirculation is evident in the numerical data but does not appear in the contour plots.) This stress decelerates the axial velocity at the surface of the rotor. By $Z/L=0.07$ (Figure 4), the $\overline{u'u'}$ value decreases with the large gradients also showing a marked reduction. The peak of the $\overline{u'u'}$ stress is transported to 110° by the tangential momentum, and the peak has diminished. Dissipation dominates the flow at this point, where upstream turbulence production is the major mechanism, and works to distribute the turbulence term fairly evenly by midplane, $Z/L=0.50$. The profile remains reasonably uniform on the suction side, but by the exit plane, $Z/L=1.00$, there are again high values of $\overline{u'u'}$. Although the gradients are steep, it seems likely that the phenomenon is real because of the circumference over which it is distributed. The turbulence producing source at this plane is the step at the end of the seal.

CONCLUSIONS

A 3-D LDA has been used to successfully measure the velocity field in a whirling annular seal. To accomplish this a number of techniques had to be used including

- * use of a transparent surface on the far side of the probe volume,
- * optical coating of all transparent surfaces,
- * special beam alignment techniques,
- * off angle (i.e. not 180°) backscatter light collection,
- * use of 8.5X beam expanders to provide a very small measurement volume,
- * use of the smallest coincidence window available at the time,
- * and use of a rotary encoder interfaced with the signal processors to permit phase information to be collected.

With the application of these techniques it was possible to measure a very complex internal flow field and to find some interesting results. At the inlet the highest axial velocities occurred in the region with the smallest clearance, forced by the upstream conditions. The axial momentum rotates the high axial velocity around the seal until it is on the opposite side by the exit, i.e. a map of maximum axial velocity traces a helix longitudinally through the seal. The radial velocities are driven by the greater axial and azimuthal velocities. As the flow separates across the inlet to the seal, the axial turbulence intensity jumps dramatically and causes the flow to decelerate. The region of maximum axial velocity fluctuations maps in a manner similar to the mean values. The exit induces another increase in the axial Reynolds stress.

The picture which develops is significantly different than is seen in an eccentric seal without the rotor whirling, Johnson [1989]. Although often experimental measurements confirm expectations developed by intuition, results such as these should provide the impetus for continued experimental measurements to ensure that erroneous assumptions about the flow fields are not adopted.

DATA AVAILABILITY

The data used for the preparation of this paper along with the entire Reynolds stress tensor are available in tabular form and on MS-DOS floppy disks.

ACKNOWLEDGEMENTS

This research was sponsored by the NASA Lewis Research Center under the supervision of Mr. Robert Hendricks and by the Texas A&M University Turbomachinery Research Consortium.

NOMENCLATURE

A	Leakage area, m^2
c	Mean clearance between the stator and rotor, m
d	Rotor diameter, m
e	Eccentricity, m
L	Length of the seal, m
Q	Leakage flow rate, m^3/s
r	Radial distance from stator centerline, m
Re	Reynolds number = $2Uc/\nu$
Ta	Taylor number = $\frac{cW_{sh}}{\nu} \sqrt{\frac{2c}{d}}$
U	Axial mean velocity, m/s
U_{ave}	Bulk mean velocity = Q/A , m/s
V	Radial mean velocity, m/s
W	Tangential mean velocity, m/s
$\overline{u'u'}$	Time averaged Reynolds stress, m^2/s^2
W_{sh}	Rotor surface speed, m/s
Z	Distance downstream of the seal inlet, m
ϵ	Eccentricity ratio, e/c
θ	Azimuthal angle measured in the direction of rotation from the minimum clearance
μ	Fluid absolute viscosity, $(N \cdot s)/m^2$
ν	Kinematic viscosity, m^2/s
ρ	Fluid density, kg/m^3
ω	Whirl ratio, ω_p/ω_r
ω_p	Rotor precession speed, rpm
ω_r	Rotor speed, rpm

REFERENCES

- Johnson, M.C., 1989, "Development of a 3-D Laser Doppler Anemometry System: With Measurements in Annular and Labyrinth Seals," Ph.D. Dissertation, Texas A&M University, College Station, Texas, 77843.
- McLaughlin, D.K. and Tiederman, W.G., 1973, "Bias Correction for Individual Realization of Laser Anemometer Measurements in Turbulent Flows," *The Physics of Fluids*, Vol. 16, pp. 2082-2088.
- Morrison, G.L., Johnson, M.C., Swan, D.L., DeOtte, R.E., 1991a, "Advantages of Orthogonal and Non-Orthogonal 3-D Anemometer Systems," *Flow Measurement and Instrumentation*, Vol. 2, pp. 89-97
- Morrison, G.L., Johnson, M.C., and Tatterson, G.B., 1991b, "Three-Dimensional Laser Anemometer Measurements in an Annular Seal," *ASME Journal of Tribology*, Vol. 113, pp. 421-427.

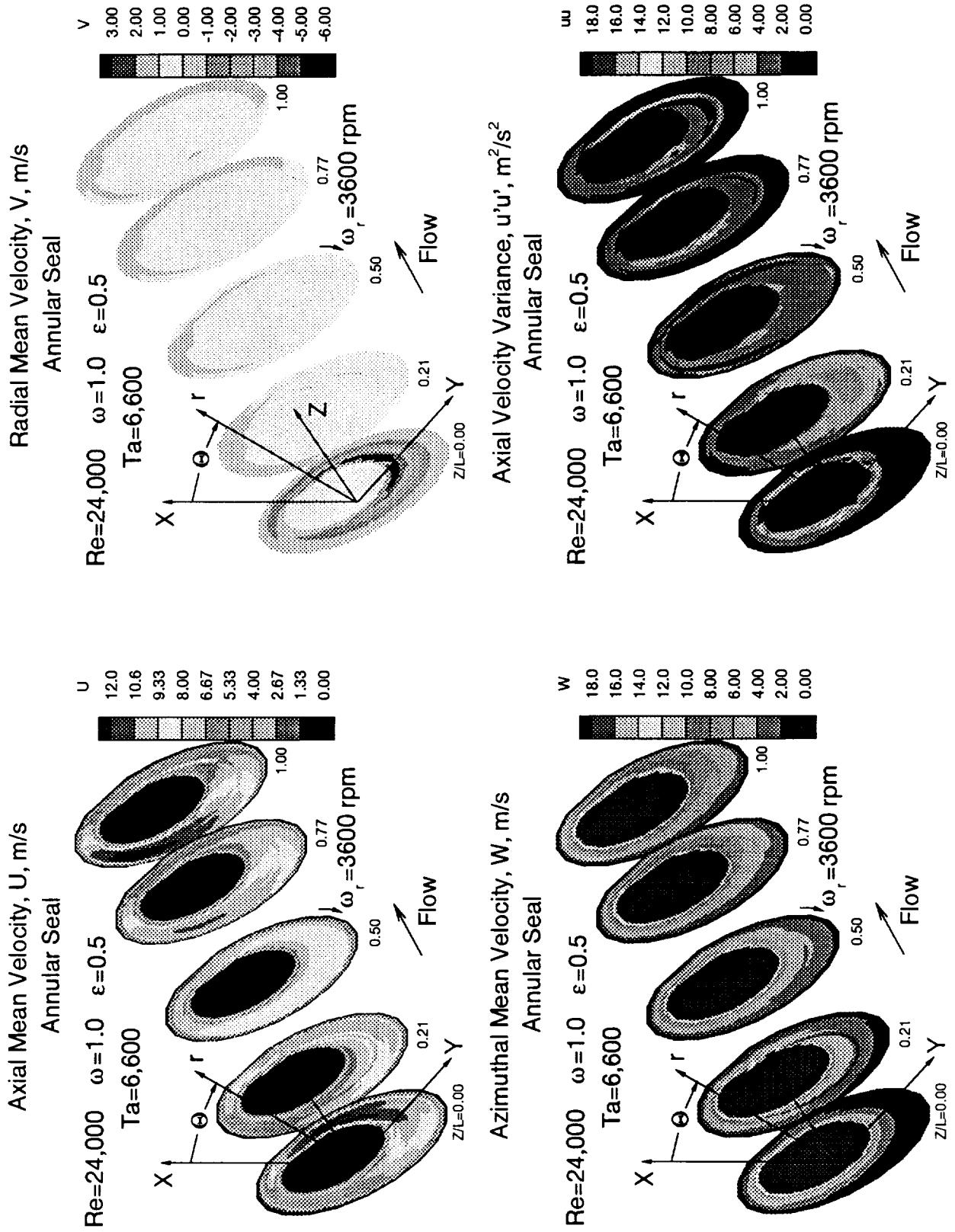


Figure 3. Mean velocity and axial velocity variance, $Re=24,000$, $0.00 \leq Z/L \leq 1.00$.

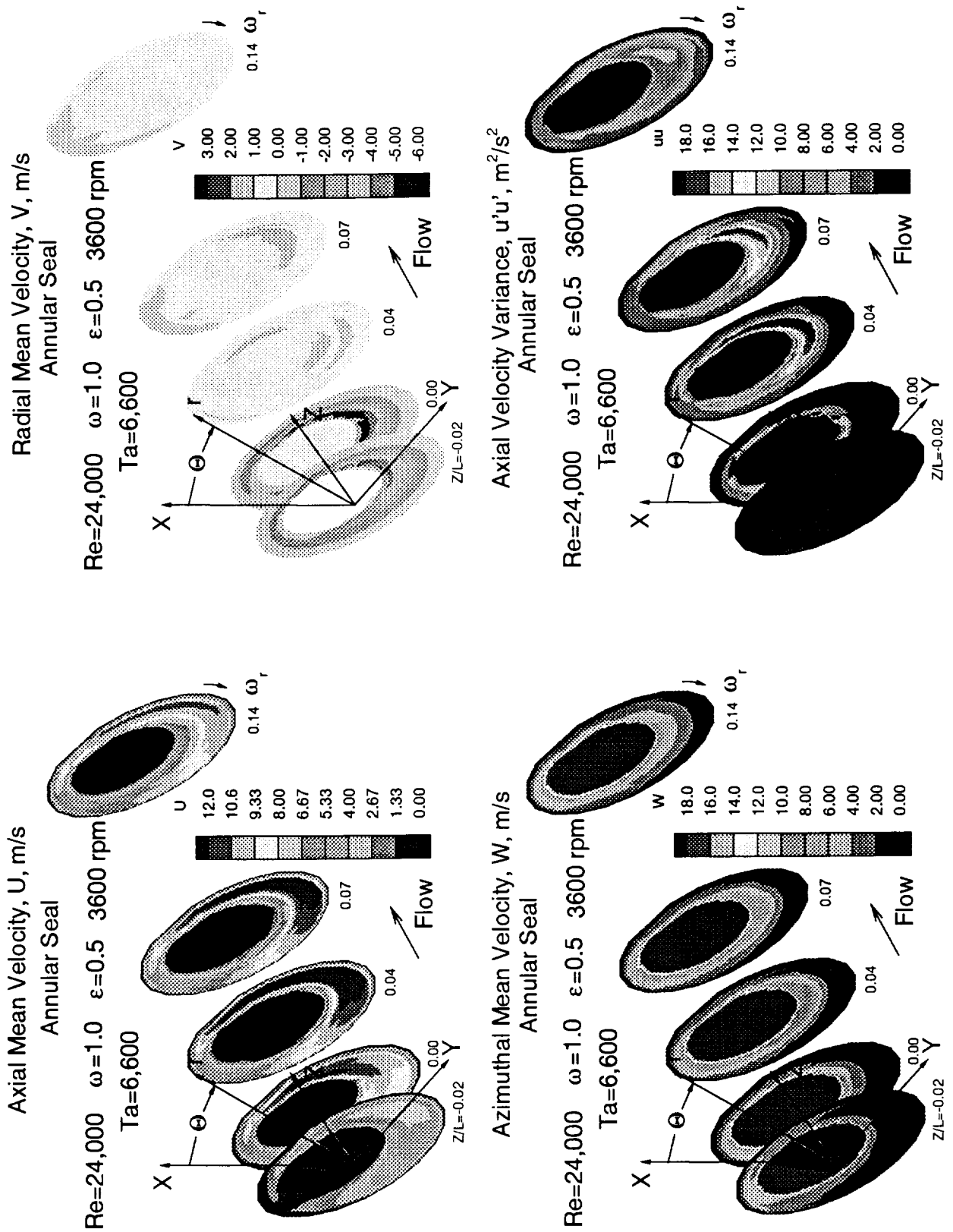


Figure 4. Mean velocity and axial velocity variance, $Re=24,000$, $-0.02 \leq Z/L \leq 0.14$.

